An Observational Study of the Evolution of Horizontal Convective Rolls

TAMMY M. WECKWERTH

Advanced Study Program and Atmospheric Technology Division, National Center for Atmospheric Research, Boulder, Colorado*

THOMAS W. HORST AND JAMES W. WILSON

Atmospheric Technology Division, National Center for Atmospheric Research, Boulder, Colorado*

(Manuscript received 10 June 1998, in final form 6 October 1998)

ABSTRACT

A comprehensive observational dataset encompassing the entire temporal evolution of horizontal convective rolls was obtained for the first time. Florida, Illinois, and Kansas measurements from preroll conditions through the development of well-defined rolls to their dissipation were utilized to determine the factors influencing roll evolution. When the buoyancy flux reached a critical value of 35–50 W m^{-2}, the first form of boundary layer convection resolved by radar was rolls. It was noted that two-dimensional convective rolls can evolve in a convective boundary layer in the absence of significant wind speed and shear. In fact, the value of wind speed or shear in itself did not seem to determine when or if rolls would form, although it did influence roll evolution. Well-defined, two-dimensional rolls only occurred while $-z_i/L$, where z_i is the convective boundary layer depth and L is the Monin–Obukhov length, was less than $\sim$25, which is consistent with previous studies. As $-z_i/L$ increased throughout the day, either open cellular convection or unorganized boundary layer convection was the dominant clear-air convective mode. If the wind speed was low (mean boundary layer winds <3 m s^{-1} or 10-m winds <2 m s^{-1}) during roll occurrences, rolls evolved into open cells. Alternatively, if the wind speed throughout the day was relatively high, rolls broke apart into random, unorganized convective elements. These are unprecedented observations of two-dimensional convection evolving into three-dimensional convection over land, which is analogous to laboratory convection where increased thermal forcing can produce a transition from two-dimensional to three-dimensional structures. Finally, the roll orientation was governed primarily by the mean convective boundary layer wind direction.

1. Introduction

Horizontal convective rolls are one of the most common forms of boundary layer convection. Laboratory and theoretical work has shown that two-dimensional rolls are the first steady-state solution of the flow field as the Rayleigh number increases beyond a critical value (e.g., Rayleigh 1916; Schlüter et al. 1965; Krishnamurti 1970; Agee 1987). This has been shown to occur with either no wind or a constant horizontal velocity as long as vertical symmetry exists (e.g., no curved temperature profile and no large-scale vertical motion). This is believed to be the first observational study of the diurnal cycle of shallow boundary layer convection that shows that rolls are the initial mode.

Previous studies have suggested that a variety of conditions may produce horizontal convective rolls. It has been shown that rolls may form in the presence of dynamical instability, including both parallel instability (e.g., Faller 1963; Lilly 1966) and inflection-point instability (e.g., Faller 1965; Brown 1972, 1980). Linear theory has also shown that rolls may exist when there is thermal instability in the presence of shear (e.g., Kuo 1963; Asai 1970a,b, 1972; Kuettner 1971). Observations, numerical models, and theoretical analyses have shown that an optimal combination of buoyancy and vertical wind shear is important for the existence of rolls (e.g., Deardorff 1972; LeMone 1973; Grossman 1982; Sykes and Henn 1989; Moeng and Sullivan 1994; Khanna and Brasseur 1998). Other dynamical conditions have been identified as necessary for roll existence: (i) a critical value of wind speed (e.g., Woodcock 1942; Malkus and Riehl 1964; Weckwerth et al. 1997), (ii) a critical value of boundary layer wind shear (e.g., Miura 1986; Sykes and Henn 1989; Weckwerth et al. 1997) and/or (iii) a unidirectional curved BL wind speed profile (Kuettner 1959, 1971; Doviak and Berger 1980).

* The National Center for Atmospheric Research is partially sponsored by the National Science Foundation.

Corresponding author address: Dr. Tammy M. Weckwerth, NCAR, P.O. Box 3000, Boulder, CO 80307-3000.
E-mail: tammy@ucar.edu

The majority of previous field projects that have observed roll occurrences were not able to obtain much data on nonroll conditions nor on the life cycle of roll occurrences (e.g., LeMone 1973; Kelly 1982, 1984; Christian and Wakimoto 1989; Miura 1986; Kristovich 1993; Weckwerth et al. 1997). Ferrare et al. (1991) showed partial evolution of linear convection starting with linear features that became less elongated due to an increase in the convective boundary layer (CBL) instability and decrease in the CBL average wind speed. Kristovich et al. (1999) identified the appearance of rolls in their wintertime lake-effect analysis region about an hour after an increase in low-level wind speed and speed shear, suggesting that increased shear was an impetus for roll formation. Other studies of rolls associated with cold air outbreak events over large bodies of water often had upstream measurements or observations within the spatial transition region between rolls and cellular convection but no measurements of the temporal evolution (e.g., Walter 1980; Kelly 1984; Brümmer et al. 1985).

Thus the goal of this study was to define the environmental parameters that induce roll formation and eventual dissipation. In order to examine the environmental conditions prior to roll formation it is essential to measure the temporal evolution of numerous parameters. It is necessary to objectively identify roll occurrences (Weckwerth et al. 1997) and measure surface layer fluxes (e.g., LeMone 1973; Christian and Wakimoto 1989; Kristovich 1993; Weckwerth et al. 1997), CBL depth (e.g., Grossman 1982; Christian and Wakimoto 1989), low-level winds (Kristovich 1993; Weckwerth et al. 1997), and CBL winds and vertical wind shear (e.g., Miura 1986). The first field project to obtain all such measurements during the entire evolution of numerous roll events was an ancillary project to the Small Cumulus Microphysical Study (SCMS) in east-central Florida during the summer of 1995. Data from two other field campaigns, that is, Flatland/Lidars In Flat Terrain (LIFT; Angevine et al. 1998; Cohn et al. 1998) in Illinois during the summer of 1996 and the Cooperative Atmosphere Surface Exchange Study (CASES-97) in Kansas during the spring of 1997, were used to address the generality of the SCMS results.

Section 2 describes the dataset and addresses issues of data quality. The factors affecting roll evolution are presented in section 3. Roll orientation is addressed in section 4. Section 5 includes a summary and conclusions.

2. The dataset

The primary dataset was obtained from the SCMS project that was conducted in east-central Florida during the summer of 1995. The observational network for this study depicted in Fig. 1 included the National Center for Atmospheric Research's (NCAR) CP-2 Doppler radar; three of NCAR's Portable Automated Mesonet (PAM III) surface stations with the newly acquired, flux-measuring capabilities (Flux-PAM); NCAR's Integrated Sounding System (ISS) including the Cross-Chain Loran Sounding System (CLASS); a 915-MHz boundary layer wind profiler and Radio Acoustic Sounding System (RASS); the University of Wyoming (UW) King Air research aircraft; a tethersonde system; and *Geostationary Operational Environmental Satellite-8* (*GOES-8*) visible satellite imagery.

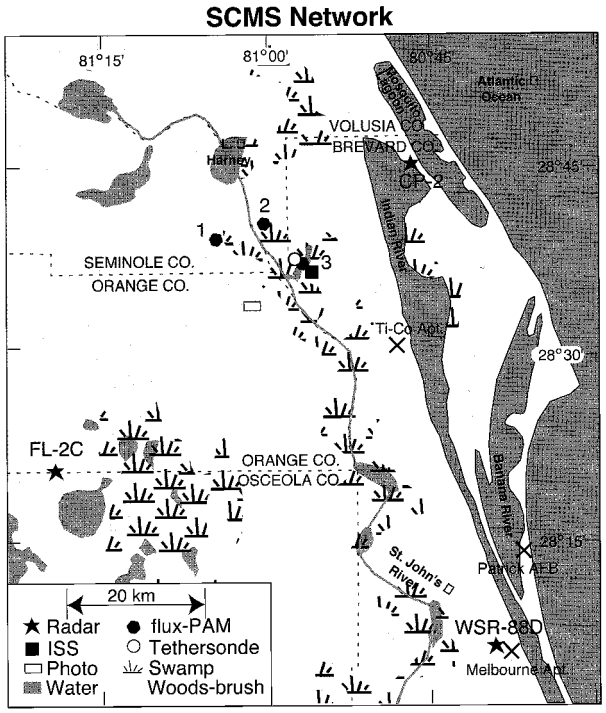

FIG. 1. Base map of SCMS observational network. The ISS, Flux-PAM 3, and tethersonde were collocated. The land type is indicated in the legend. The white areas depict flat, relatively dry regions. The ×'s mark the locations of airports.

a. Radar

Data from the CP-2 radar's (Keeler et al. 1989) final field deployment during SCMS were used to ascertain the organization of the boundary layer convective motions. Significant ground clutter was a factor at low levels within approximately 10 km toward the west, but good data were obtained over the ISS and Flux-PAM sites where the environmental measurements were collected. Sector scans over the surface station network were nominally collected every 10 min with a gate spacing of 150 m. The Doppler on Wheels (DOW1; Wurman et al. 1995) mobile 3-cm radar was utilized during the Flatland/LIFT project while NCAR's new S-band (10 cm) polarimetric (S-Pol; Lutz et al. 1997) radar was used during CASES-97.

Clear-air return at X band (3 cm) is less contaminated by ground clutter than S band (Wilson et al. 1984); thus, the CP-2 X band was used to define the convective

motions. In a pattern-recognition scheme similar to that described in Fankhauser et al. (1995), a two-dimensional correlation analysis was used to quantify the linearity of the reflectivity field. Although not perfect, the motivation for using this technique was to be objective in defining rolls, their orientation, and wavelength. For each range–azimuth grid point a correlation between the radar reflectivity field and a linear cosine wave was obtained. A cosine function of the form $\cos(2\pi x/\lambda)$ was used where x is the distance in the cross-roll direction from the range-azimuth grid point to the subsequent grid point and λ is the specified wavelength of the rolls. The correlation analysis was performed over one wavelength in the cross-roll direction with the peak of the cosine wave corresponding to the gridpoint location. The analysis was done over some specified length (4 km in this case) in the along-roll direction. Several analyses were performed with different wavelengths (0.5–2 km) and the roll wavelength was defined as that which produced the maximum correlation. At each data point, the roll orientation was determined by rotating the axis of the linear cosine wave through numerous discrete angles and finding the orientation of maximum correlation between the cosine function and the reflectivity field. The fraction of the area with correlation coefficients greater than 0.2 was arbitrarily chosen to be used as a measure of the linear convective organization. This pattern-recognition scheme produced similar results to the spatial autocorrelation technique in Weckwerth et al. (1997) but had the advantage of working in polar coordinates thus not requiring interpolation of radar data onto a Cartesian grid. This scheme could produce different results in different regions of the reflectivity field but care was taken to analyze the same region throughout an entire day's evolution.

These correlation analyses were performed only on the SCMS dataset. The procedure was not effective with the DOW1 data during Flatland/LIFT due to difficulties with the scan control software, which frequently resulted in oscillating elevation angles. There were no X-band data available during CASES-97; thus, the clear-air return was quite noisy due to ground clutter contamination and a direct objective comparison with the SCMS dataset was not possible. Although data from Flatland/LIFT and CASES-97 will be shown, they were not analyzed quantitatively as were the SCMS radar data.

b. Flux-PAM stations

While SCMS was the final field project for CP-2, it was the first deployment of the Flux-PAM stations (Militzer et al. 1995; Horst and Oncley 1995). The Flux-PAM stations collected 5-min measurements of buoyancy and momentum fluxes, as well as 1-min samples of temperature, moisture, winds, pressure, rainfall, and radiation measurements. The sites were chosen to be representative samples of the terrain over which the rolls were observed by CP-2, as well as to have uniform upwind fetch for at least 100 times the 3-m measurement height (Horst and Weil 1994). Flux-PAM station 1 was in the middle of a grassy pasture. Flux-PAM station 2 was sited in a grassy wetlands area. After Hurricane Erin passed through the region on 1 August 1995, however, the site was flooded. Flux-PAM station 3 was collocated with the ISS and the tethersonde on a dike between two lakes with tall grass along the shores and was therefore classified as wetlands. The data from all Flux-PAM stations have been corrected for minimal tilts of the sonic anemometers. These Flux-PAM stations were also deployed for the Flatland/LIFT and CASES-97 projects.

c. ISS

Two capabilities of ISS (Parsons et al. 1994) were extensively utilized during SCMS: CLASS radiosonde launches (Lauritsen et al. 1987) and the 915-MHz boundary layer wind profiler. Radiosondes were launched two to four times each day and have been quality corrected for sensor arm heating (Miller and Riddle 1994). Vertical profiles of horizontal winds were inferred from the profiler data every 30 min when the system was operational. The signal-to-noise ratio of the profiler was used to define the CBL depth (e.g., Angevine et al. 1994). These values were consistently within 100 m of the corresponding radiosonde CBL depth estimates. An NCAR ISS was deployed during Flatland/LIFT. For CASES-97, Argonne National Laboratory operated three 915-MHz profilers within their Argonne Boundary Layer Experiments (ABLE) array. At each ABLE profiler site, there is also a minisodar that extends the wind profiles down closer to the surface than is typical for the ISS.

d. UW King Air

Approximately 12 h of King Air flight time were utilized to examine the representativeness of the surface Flux-PAM sites in SCMS. One of the flight patterns used legs at two heights: 200 and 700 m alternately measuring fluxes over the St. John's River basin and over the wooded regions. Another flight pattern consisted of legs at several different heights within the CBL across both the river basin and woods to provide integrated flux measurements. All flight legs utilized in the analyses were from the cross-wind direction. This corresponded to flying across rolls when they were present.

Note the varied terrain measured by the Flux-PAMs in Fig. 1 including relatively dry areas, swamp land, and open water. It was hoped that the separate flight legs over the river basin and over the woods would help to ascertain the relative influence of the water and the woods to the overall flux measurements. An appropriate spatial weighting scheme for the Flux-PAM stations could then be determined. Unfortunately, 12 flight hours

were insufficient to address this issue. Buoyancy fluxes from the flights across both the river and the woods, however, did compare favorably (within 5%) with an average of the surface Flux-PAM station data.

e. Tethersonde system

A tethersonde system from A.I.R., Inc. was leased for the duration of the SCMS. Sondes were typically flown at 10, 20, 40, 80 and 120 m above ground level (AGL) throughout the project. The primary motivation for utilizing the tethersonde was to obtain low-level wind measurements below the lowest profiler gate. Due to optimal siting of the ISS and the high water vapor content of the air, however, plausible wind profiler data were obtained as low as 60 m AGL during SCMS. Winds measured by the tethersonde will be shown for validation and comparison with the Flux-PAM and profiler data. Calibrations within NCAR's wind tunnel showed that the tethersonde wind speeds were accurate to 0.4 m s^{-1} and wind direction to within 10°. Temperature chamber measurements obtained from the tethersonde were also of high quality. They were accurate to within 0.6°C. Relative humidity measurements, however, were unacceptable due to the inaccuracy of the sensors, which was often as high as 30%. Tethersonde measurements were not obtained during Flatland/LIFT or CASES-97.

3. Roll evolution

A complete time history of roll evolution utilizing data from all instruments was obtained on 14 August 1995 during SCMS and will therefore be shown in detail. The entire evolution was also obtained on several other days during SCMS, Flatland/LIFT, and CASES-97, although all instruments were not available. These data will be shown as appropriate to add to the generality of the results.

a. Boundary layer convective motions

The visible satellite imagery showed no evidence of cumulus clouds near the SCMS surface station network (black box in Fig. 2) at 1030 LT on 14 August 1995 (LT = UTC − 4 h during SCMS). By 1115 LT (Fig. 2b) the westward propagation of the east-coast seabreeze front (SBF) was apparent as were northwest–southeast- and north–south-oriented cloud streets, which are indicative of rolls occurring within the CBL. The cloud field in advance of the SBF became less organized by 1300 LT (Fig. 2c) and was broken up even further by 1415 LT (Fig. 2d).

The X-band radar reflectivity field at 0908 LT on 14 August 1995 (Fig. 3a) shows some fairly large regions of relatively stronger reflectivities that were likely due to large concentrations of insects. The reason for the sporadic concentration of insects in varied regions is unknown but it is clear that there were no organized convective structures. At 0940 LT (Fig. 3b), prior to the formation of cloud streets (see Fig. 2), there was a suggestion of north-northwest–south-southeast-oriented linear features. This is evident in the tightly spaced yellow bands of enhanced reflectivity 15–25 km west-southwest of CP-2. The daytime heating created a CBL in which insects were the primary scattering mechanisms (Wilson et al. 1994). Note that the first form of organized boundary layer convection that was apparent in the radar data is two-dimensional roll convection aligned along the mean wind direction (see Flux-PAM wind directions on Fig. 3b). By 1025 LT (Fig. 3c) these rolls were well defined with a spacing (aspect ratio) of approximately 1 km (1.4). Note that even though well-defined rolls existed at this time, there were still no cloud streets observed in the satellite imagery (Fig. 2a). At 1126 LT (Fig. 3d) when the cloud streets were apparent (Fig. 2b), the wavelength (aspect ratio) of the rolls was 1.5 km (1.1). A higher elevation angle (0.8°) is shown for the later times to display the reflectivity field near the middle of the CBL. The diminished convective motions over and downwind from Lake Harney (about 27 km west of CP-2) were probably due to downwind subsidence and a suppressed CBL (e.g., Rabin et al. 1990; Segal et al. 1997). As the sea-breeze front was passing over Flux-PAM stations 2 and 3 at 1316 LT (Fig. 3e), the prefrontal, radar-observed convective features were not as elongated and linear, but rather unorganized, similar to that shown in the satellite imagery (Fig. 2c). The postfrontal Flux-PAM, CP-2, and ISS measurements were not used in the roll evolution analyses.

The evolution of radar data on 24 July and 7 August 1995 during SCMS is shown in Figs. 4 and 5, respectively. Similar to 14 August (Fig. 3) both days commenced with no apparent convective features visible in the radar images. At 0923 LT on 24 July 1995 northeast–southwest-oriented linear bands with a spacing (aspect ratio) of 0.7 km (2.3), indicative of rolls, were apparent in the radar data (Fig. 4b). By 1058 LT (Fig. 4c) the spacing (aspect ratio) was 1 km (1.8). At 1328 LT there were some streaks or linearity in the reflectivity field but overall, the boundary layer was dominated by unorganized convective elements (Fig. 4d). At 0945 LT on 7 August 1995 northeast–southwest two-dimensional bands with a wavelength (aspect ratio) of 0.7 km (2.1) were observed by the radar (Fig. 5b). The spacing (aspect ratio) had increased to 1 km (2.5) at 1034 LT and the orientation had changed slightly as the rolls were starting to break apart (Fig. 5c). Figure 5d at 1126 LT shows that the rolls evolved into a field of open cellular structures (e.g., Agee 1987).

Similarly the DOW1 radar data from Illinois during the Flatland/LIFT project on 13 August 1996 showed no apparent convective features at 0832 LT (Fig. 6a; LT = UTC − 5 h during Flatland/LIFT) and at 0914 LT (Fig. 6b) there were northwest–southeast-oriented linear bands with a wavelength of 0.5 km. The aspect ratio

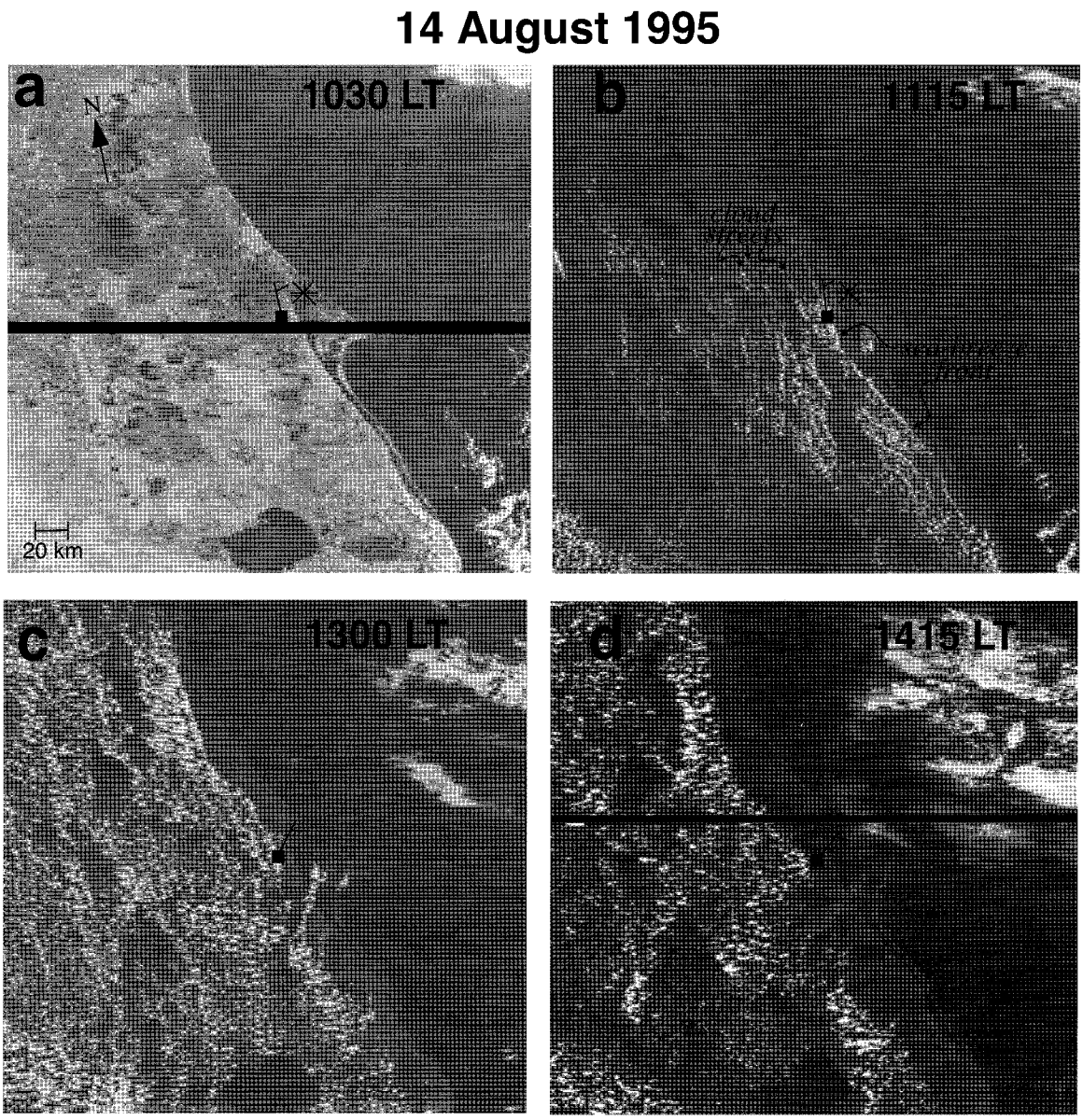

FIG. 2. *GOES-8* visible satellite imagery at (a) 1030, (b) 1115, (c) 1300, and (d) 1415 LT 14 Aug 1995 during SCMS. Half barb is 2.5 m s^{-1} wind from the ISS/Flux-PAM 3/tethersonde site. Star indicates location of CP-2 and the box is the location of the ISS/PAM 3/tethersonde site. The horizontal black stripes in (a) and (d) indicate missing or bad scan lines.

could not be determined at 0914 LT due to the immeasurable, shallow CBL depth. These linear roll-like features were only apparent within a couple of kilometers surrounding the radar due to their shallowness and the relatively high elevation angle (1.2°) necessary to scan above the ground clutter. The spacing (aspect ratio) increased to 1 km (1.6) at 1110 LT as the rolls became less linear (Fig. 6c). Open cellular convection was observed at 1133 LT (Fig. 6d). It is apparent that the clear-air echoes from DOW1 were weaker than those obtained from CP-2. This may have been due to a lack of an absolute calibration with DOW1. It is believed, however, that the relative magnitudes of reflectivity are accurate. Thus the clear-air enhancements are representative of boundary layer convective motions.

Although the S-band clear-air return was weak at 0800 LT (LT = UTC − 5 h during CASES-97) on 4 May 1997 in Kansas, there were no discernible convective features (not shown). Northeast–southwest rolls with a 0.8-km wavelength (aspect ratio of 4) were visible by 0900 LT. The spacing (aspect ratio) was 2 km (1.7) at 1230 LT and the rolls broke apart into unorganized convective elements by 1430 LT (not shown).

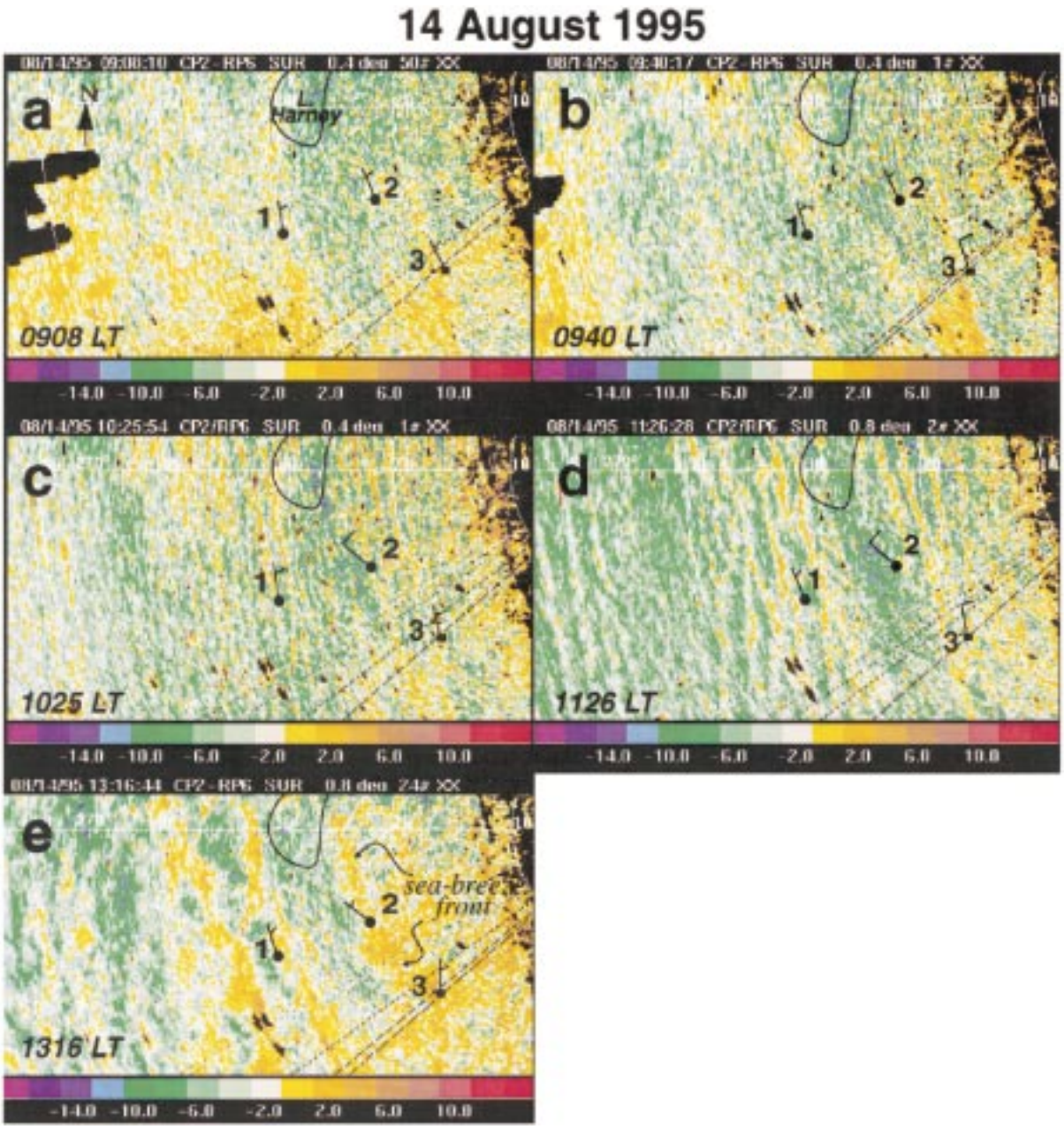

FIG. 3. Time series of CP-2 X-band reflectivity field (dBZ$_e$) on 14 Aug 1995 during SCMS at (a) 0908, (b) 0940, (c) 1025, (d) 1126, and (e) 1316 LT. Black regions indicate bad data. The Flux-PAM winds are shown with a half barb indicating 2.5 m s^{-1} and a full barb depicting 5 m s^{-1}. Range rings are every 10 km; azimuth lines are every 30°. The outline of Lake Harney is shown for reference.

b. Roll formation

In all examples examined (14 August 1995, 27 July 1995, 11 August 1995, 13 August 1996, and 4 May 1997) from three locations (Florida, Illinois, and Kansas), it was striking that *the initial form of organized boundary layer convective features resolved by the radar was two-dimensional rolls.* This was also observed in all other analyzed cases in which data were obtained during the formation of boundary layer convective motions (eight other case studies from SCMS). An examination of the impetus for the onset of convection will be presented in section 3b(2).

1) EVIDENCE OF ROLLS

The question arises as to how well the radar can detect the convective features on which this paper is focused, namely rolls. The ability of radar to observe kinematic

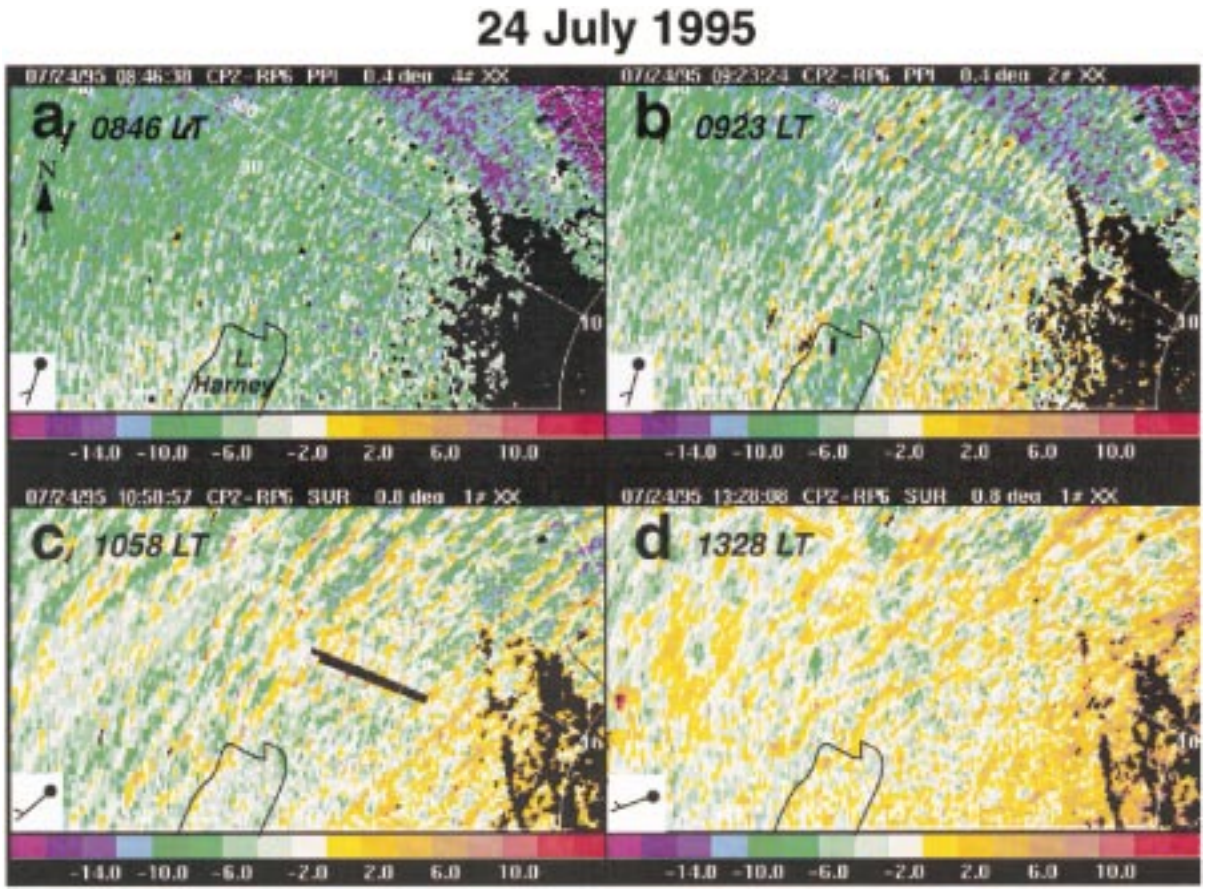

FIG. 4. Time series of CP-2 X-band radar reflectivity data (dBZ_e) on 24 Jul 1995 during SCMS. Times shown are (a) 0846, (b) 0923, (c) 1058, and (d) 1328 LT. Black regions indicate bad data. Surface station network is ~5 km to the south of these images. Average value of surface station winds is shown in the lower-left corner of each image. Half barb is 2.5 m s^{-1}. Range rings are every 10 km; azimuth lines are every 30°. The outline of Lake Harney is shown for reference.

features in the clear-air boundary layer, and in particular horizontal convective rolls in Florida, has been addressed in detail by Wilson et al. (1994) and Russell and Wilson (1996). Conclusions from their research relevant to this study are as follows: (i) when the surface temperature is greater than 10°C, the predominant scattering mechanism in the CBL is insects; (ii) the insects are passive tracers of horizontal motion and therefore ideal targets for remotely detecting wind patterns in the clear-air boundary layer; (iii) enhanced thin lines of clear-air reflectivity correspond to regions of updrafts; and (iv) kinematic details of rolls can be determined from Doppler radar.

In the aforementioned studies, the data were obtained after the onset of rolls. It is as yet unclear if there was indeed an absence of convective motions within the boundary layer when the radar did not depict any organized clear-air enhancements in the reflectivity field. This issue was partially addressed with the SCMS dataset. There was one early morning King Air flight on 27 July 1995 prior to the radar observation of rolls. This flight was contrasted with aircraft data obtained on 14 August when the radar depicted well-defined rolls (near the time of Fig. 3d). The CP-2 enhanced radar reflectivity regions greater than 0 dBZ_e (like those apparent in Fig. 3d) are shaded in Fig. 7a. The radar-observed thin lines associated with rolls were determined subjectively and are depicted as R's in Fig. 7a. These regions were generally correlated with maxima in the aircraft-measured vertical motion and mixing ratios. At 232 m ($0.3z_i$) the mixing ratio and vertical velocity variations were, respectively, 1–2 g kg^{-1} and 2 m s^{-1} between roll updraft and downdraft branches, consistent with the results of Weckwerth et al. (1996). In addition, roll updraft branches had relatively higher values of buoyancy fluxes (not shown) and were correlated with local maxima in virtual potential temperatures, indicating that the rolls were a form of thermal convection. This, along with the fact that there was very little shear across and atop the CBL, is evidence that they were not forced by gravity waves aloft (e.g., Clark et al. 1986).

In contrast on an early morning flight on 27 July 1995 when no convective features were apparent in the radar data (not shown but similar to Fig. 4a), the flight leg at

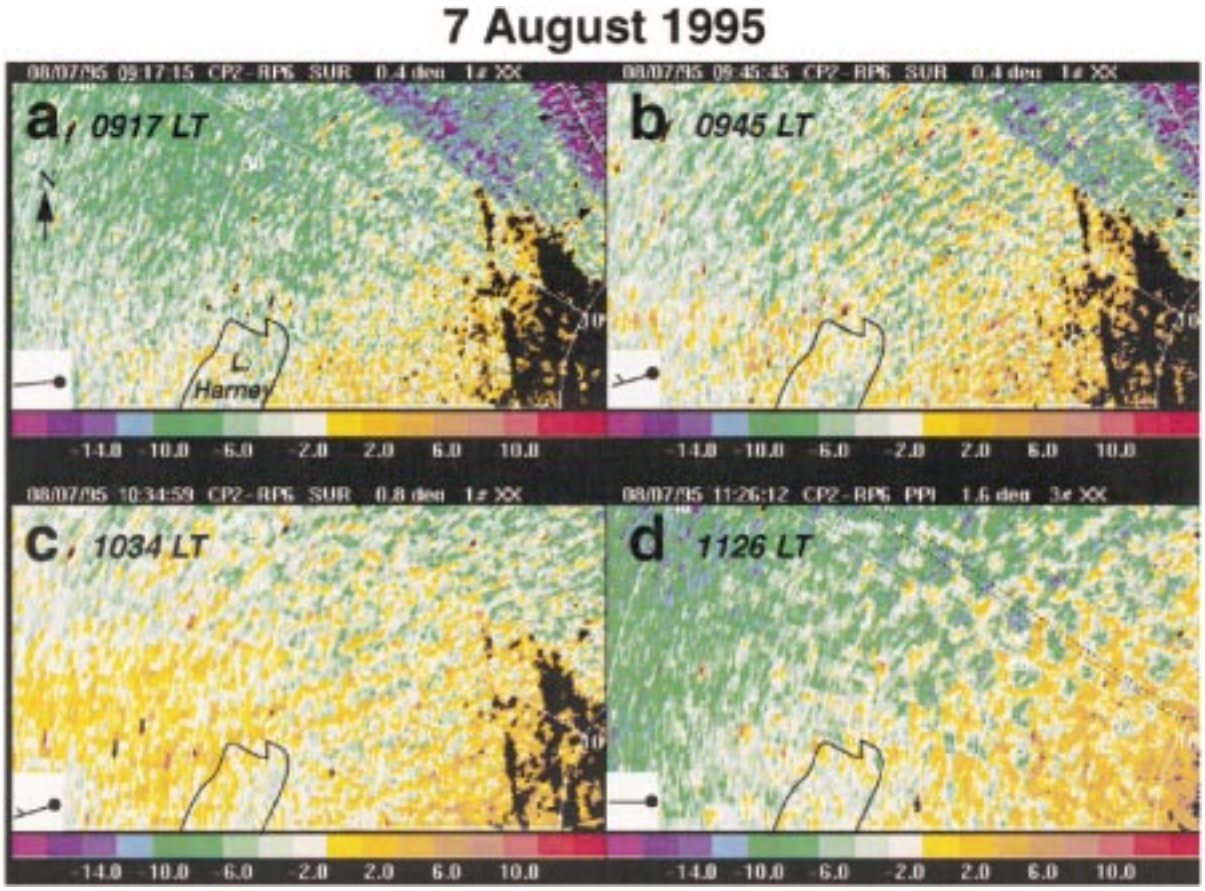

FIG. 5. Time series of CP-2 X-band radar reflectivity data (dBZ_e) on 7 Aug 1995 during SCMS. Times shown are (a) 0917, (b) 0945, (c) 1034, and (d) 1126 LT. Black regions indicate bad data. Surface station network is ~5 km to the south of these images. Average value of surface station winds is shown in the lower-left corner of each image. Half barb is 2.5 m s^{-1}. Range rings are every 10 km; azimuth lines are every 30°. The outline of Lake Harney is shown for reference.

170 m showed no obvious convective features (Fig. 7b). The mixed layer was not yet developed at this early hour and thus the height relative to the boundary layer depth could not be measured. Note that the vertical motions were negative and the variations were of much smaller magnitude than those in Fig. 7a. While large spatial variations in mixing ratio existed they were not related to convection at this time. Higher-elevation flight legs showed even less variability and a more quiescent field than at 170 m. There were no cross-wind flight legs below 170 m on this day. Thus, the aircraft data support the radar indication of no convective features at this time.

This does not rule out the possibility that very shallow (<200 m), small-scale (<1 km) convective features exist prior to the radar detection of rolls. However, the fact that the aircraft and radar both showed definitive roll signatures on 14 August 1995 and both showed the nonexistence of rolls on 27 July 1995 is supporting evidence of the radar's ability to define these convective structures.

2) IMPETUS FOR ROLL FORMATION

Past theoretical and laboratory research has shown that a critical Rayleigh number must be achieved prior to the onset of convection (e.g., Rayleigh 1916; Chandrasekhar 1961; Goldstein and Graham 1969). Furthermore, other studies suggest that rolls should be the first mode of convection as the Rayleigh number increases beyond its critical value. This was shown to occur in the absence of vertical asymmetry with either no flow or with a constant horizontal flow (e.g., Malkus 1954; Schlüter et al. 1965; Krishnamurti 1970; Agee 1987). The atmospheric Rayleigh number (Ra) is defined as

$$\mathrm{Ra} = \frac{g\Delta\theta z_i^3}{\overline{\theta} k_M k_H},$$

where g is gravitational acceleration, $\overline{\theta}$ is the mean CBL potential temperature, $\Delta\theta$ is the potential temperature difference across the CBL, z_i is CBL depth, and k_M and k_H are the eddy diffusivities for momentum and heat, respectively.

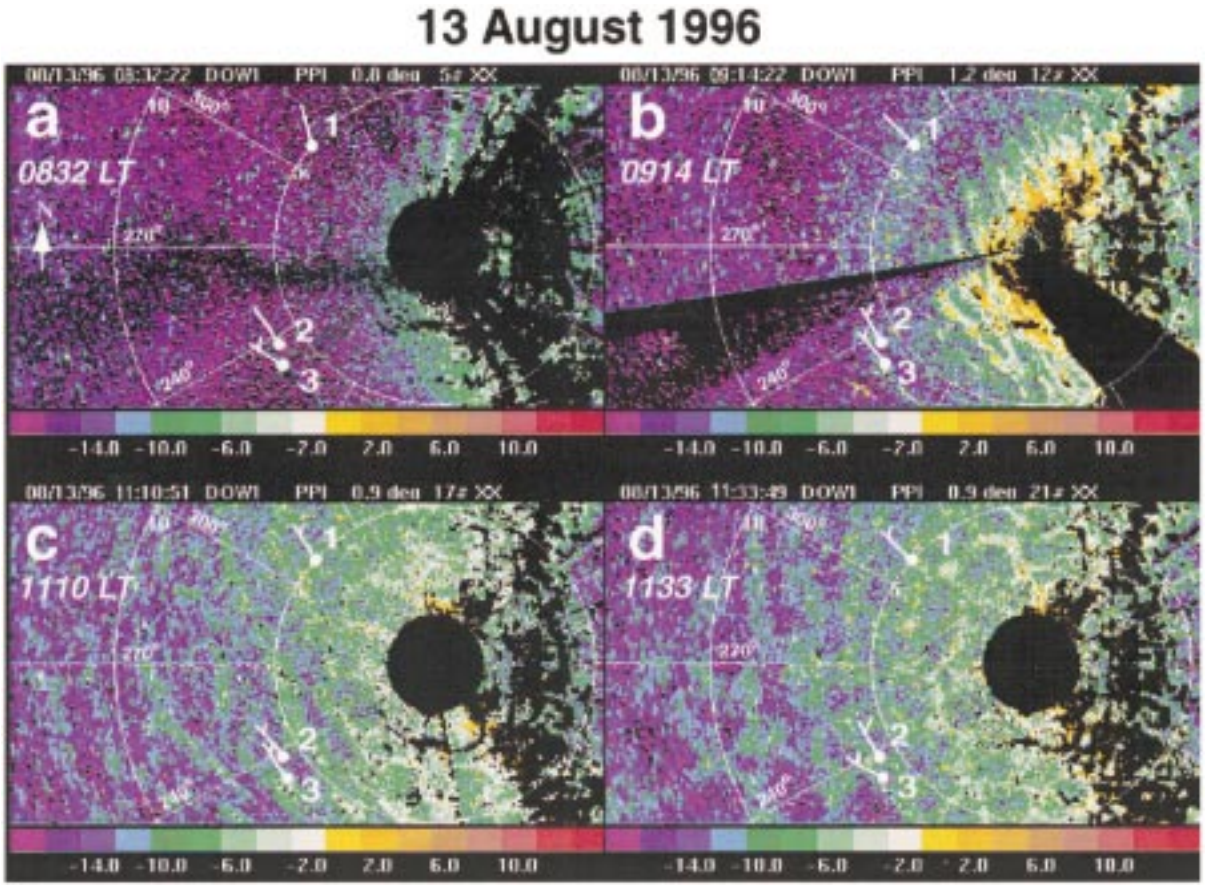

FIG. 6. Time series of DOW1 X-band radar reflectivity data (dBZ_e) on 13 Aug 1996 during Flatland/LIFT in Illinois. Times shown are (a) 0832, (b) 0914, (c) 1110, and (d) 1133 LT. Black regions indicate bad data. The ISS was collocated with the radar. The wind measurements from the three Flux-PAM stations are shown. Half barb is 2.5 m s^{-1}. Range rings are every 5 km; azimuth lines are every 30°.

Unfortunately the virtual temperature profiles from RASS were very noisy for this dataset. Thus the time series of Rayleigh numbers could not be calculated. Alternate datasets were used to examine the thermodynamic evolution of the CBL. Figure 8 shows the sounding evolution on 14 August 1995. At 0819 LT (Fig. 8a) there was a 200-m-deep surface-based stable layer topped by a residual layer from the previous day's CBL up to 1.2 km, which was further capped by a dry, stable layer. The low-level winds were northwesterly at 2.5–5 m s^{-1} veering to northeasterly above 1.2 km. At 1050 LT, the CBL depth, defined as the layer with constant equivalent potential temperature (not shown), was about 700 m deep and the residual layer remained evident up to 1.1 km. The winds were similar to those at 0819 LT (Fig. 8a). At 1120 LT (Fig. 8b) the residual layer was still evident as the CBL had grown to 800 m. The winds were not varying significantly. By 1309 LT the residual layer was completely mixed out as the CBL had grown to 1.3 km and the winds were northeasterly throughout the balloon's ascent. The radiosonde likely penetrated a cloud atop a roll updraft (Weckwerth et al. 1996) as evidenced by the region of near 100% relative humidity from 1.3 to 2.1 km. The sonde exited into a dry, stable layer.

Figure 9 shows a time series of ISS wind profiler data on 14 August 1995. The winds were consistent with the soundings of Fig. 8. In addition, the range-corrected signal-to-noise ratio (SNR) from the profiler is contoured in Fig. 9. The maxima in SNR identified the top of the CBL where the index of refraction gradients were the strongest (e.g., Angevine et al. 1994). This method provided a continuous estimate of CBL depth throughout the day. The values suggested by the profiler (dashed line) correspond well with those measured by the balloon sounding (black dots). The rapid growth of the CBL was consistent with the classic CBL growth (Stull 1988; Garratt 1992). The maxima in SNR at 1.1–1.2 km between 0800 and 1100 LT were caused by the residual layer, which was also apparent in the soundings (Fig. 8a). The enhanced return at 2.0 km between 1220 and 1440 LT was likely due to cumulus clouds passing overhead, consistent with the 1309 LT sounding (Fig. 8b), which suggested a cloud penetration near 2.0 km. Note that the capability of defining the depth of the well-mixed layer (i.e., 0930 LT) corresponded with the time

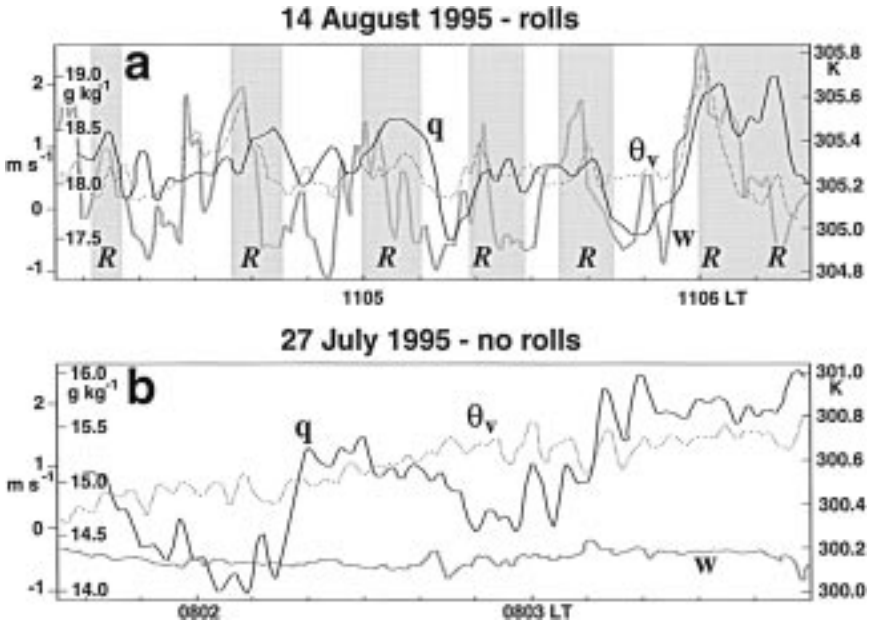

FIG. 7. The UW King Air measurements of vertical velocity (m s^{-1}; gray lines), mixing ratio (g kg^{-1}; solid black lines), and virtual potential temperature (K; dotted lines). Measurements were taken in the cross-wind direction during (a) roll occurrences on 14 Aug 1995 and (b) no radar-observed convective features on 27 Jul 1995 during SCMS. Flight levels were (a) 232 m AGL or $0.3z_i$ and (b) 170 m AGL (there was not a well-defined mixed layer at this early time). Gray shadings indicate times the King Air passed through CP-2 radar reflectivity values greater than 0 dBZ_e. The *R*'s depict subjectively determined roll updraft features as observed by the radar.

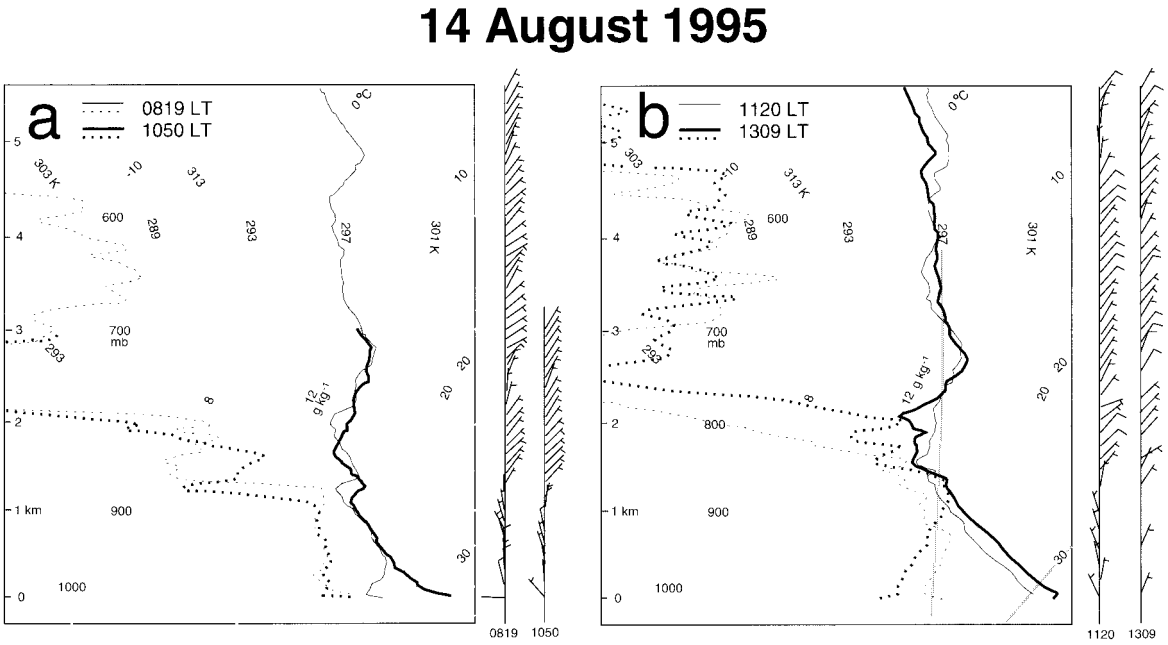

FIG. 8. Soundings on 14 Aug 1995 at (a) 0819, 1050, (b) 1120, and 1309 LT. Solid lines depict temperature and dashed lines depict dewpoint temperature traces. Horizontal wind speeds are shown on the right (full barb is 5 m s^{-1}; half barb is 2.5 m s^{-1}).

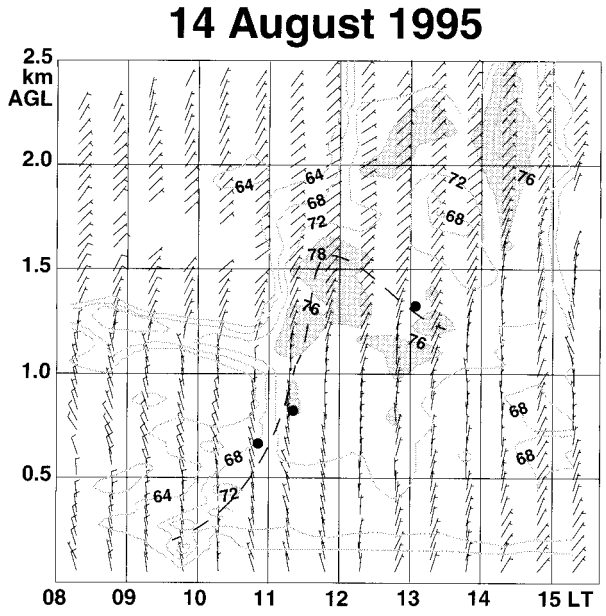

FIG. 9. Time series of wind profiler data on 14 Aug 1995 during SCMS. Full barbs are 5 m s^{-1} and half barbs are 2.5 m s^{-1}. Gray contours are range-corrected SNR every 4 dB starting at 64 dB with values greater than 76 dB shaded. The approximate height of the CBL, as determined from the maximum in SNR, is shown as the dashed line. The CBL height from the three latest CLASS soundings of Fig. 8 are shown as black dots.

at which convection was observed by the radar. Prior to the development of a well-mixed CBL, the appropriate definition of z_i was unknown.

Figure 10 shows the evolution of linear convective organization (as defined by the correlation analysis technique described in section 2a) along with various wind speed and shear measurements. The mean CBL wind speed was an average over the entire CBL as measured by the profiler. The CBL shear was taken between the profiler wind measurement at the top of the CBL and the Flux-PAM 10-m wind measurement. The low-level wind speed was the profiler mean across the lowest 200 m while the low-level shear was taken between the profiler measurement at 200 m and the Flux-PAM 10-m wind. The tethersonde wind speed was an average in the lowest 120 m when the tethersonde was operational and the tethersonde shear was the shear between the 120- and 10-m sondes. The Flux-PAM wind speed was measured at 10 m. The magnitude of wind speed did not seem to be influential in the production of rolls (Fig. 10). As the linear convective organization was increasing during SCMS, the mean CBL wind speed and the low-level profiler wind speed were either decreasing (Figs. 10a and 10c) or remaining constant (Fig. 10e). The tethersonde and Flux-PAM winds varied minimally throughout the day. Some of the previous observational studies have suggested that there is a minimum wind speed criterion that must be met for rolls to exist (e.g., Woodcock 1942; Malkus and Riehl 1964; Weckwerth et al. 1997). These data do not eliminate the possibility of a minimum wind speed threshold for roll occurrences but that value would have to be very small (i.e., mean CBL wind speed ~2 m s^{-1} or 10-m wind speed ~1 m s^{-1}).

Although the three shear measurements on 14 August 1995 suggested similar trends during roll evolution (Fig. 10b), this was not apparent on the other days examined. Consistent with the results of Miura (1986) and Weckwerth et al. (1997), however, rolls occurred only when the CBL shear was greater than approximately 10^{-3} s^{-1}. When this shear value was not met (i.e., 1300 LT on 14 August 1995, 1200 LT on 24 July 1995, and 1220 LT on 13 August 1996), linear convection was no longer apparent in the radar data. It should be noted that this value is minuscule and it is uncommon to observe CBL shear smaller than 10^{-3} s^{-1}. The shear curvature (i.e., change in shear with height) was also measured and was often, but not always, greater than the threshold of 10^{-6} to 10^{-7} cm^{-1} s^{-1} suggested by Kuettner (1959, 1971).

Thus although all of these observations of rolls occurred with some wind and shear, the magnitudes were minimal. There did not appear to be wind speed or shear threshold values that dictated when or if rolls would form. In addition, the trend in wind speed and shear did not consistently affect the entire evolution of rolls.

A nondimensional parameter commonly used to quantify the stability of the CBL, including both z_i and surface layer fluxes, is $-z_i/L$, where L is the Monin–Obukhov length, as given by Stull (1988):

$$L = \frac{\overline{-T_v}(\overline{u'w'_s}^2 + \overline{v'w'_s}^2)^{0.75}}{kg\overline{w'T'_{v_s}}}.$$

The overbars represent the temporal mean values, the subscript s represents near surface values, T_v is the virtual temperature, $\overline{u'w'}$ and $\overline{v'w'}$ are the kinematic momentum fluxes, k is the von Kármán constant, g is gravitational acceleration, and $\overline{w'T'_v}$ is the kinematic buoyancy flux. With a three-dimensional numerical model, Deardorff (1972) demonstrated that longitudinal rolls would exist within slightly unstable convective boundary layers (i.e., $0 \leq -z_i/L \leq 4.5$). Grossman (1982) observationally recorded roll existence within environments of $-z_i/L < 21.4$, and LeMone (1973) observed rolls when $3 \leq -z_i/L \leq 10$. Similarly, Sykes and Henn (1989) simulated rolls only when $-z_i/L < 9.3$. Other studies, however, have observed rolls with $-z_i/L > 136$ (Christian and Wakimoto 1989; Ferrare et al. 1991; Kristovich 1993).

For all five days presented, early in the morning when the CBL depth was shallow, $-z_i/L$ was small (Fig. 11). This parameter was small throughout the morning and did not achieve a measurable threshold before rolls formed. Thus $-z_i/L$ was not useful in explaining the *formation* of rolls. Small values of $-z_i/L$ may have been a necessary but not a sufficient condition for rolls to form. Furthermore very early in the morning prior to

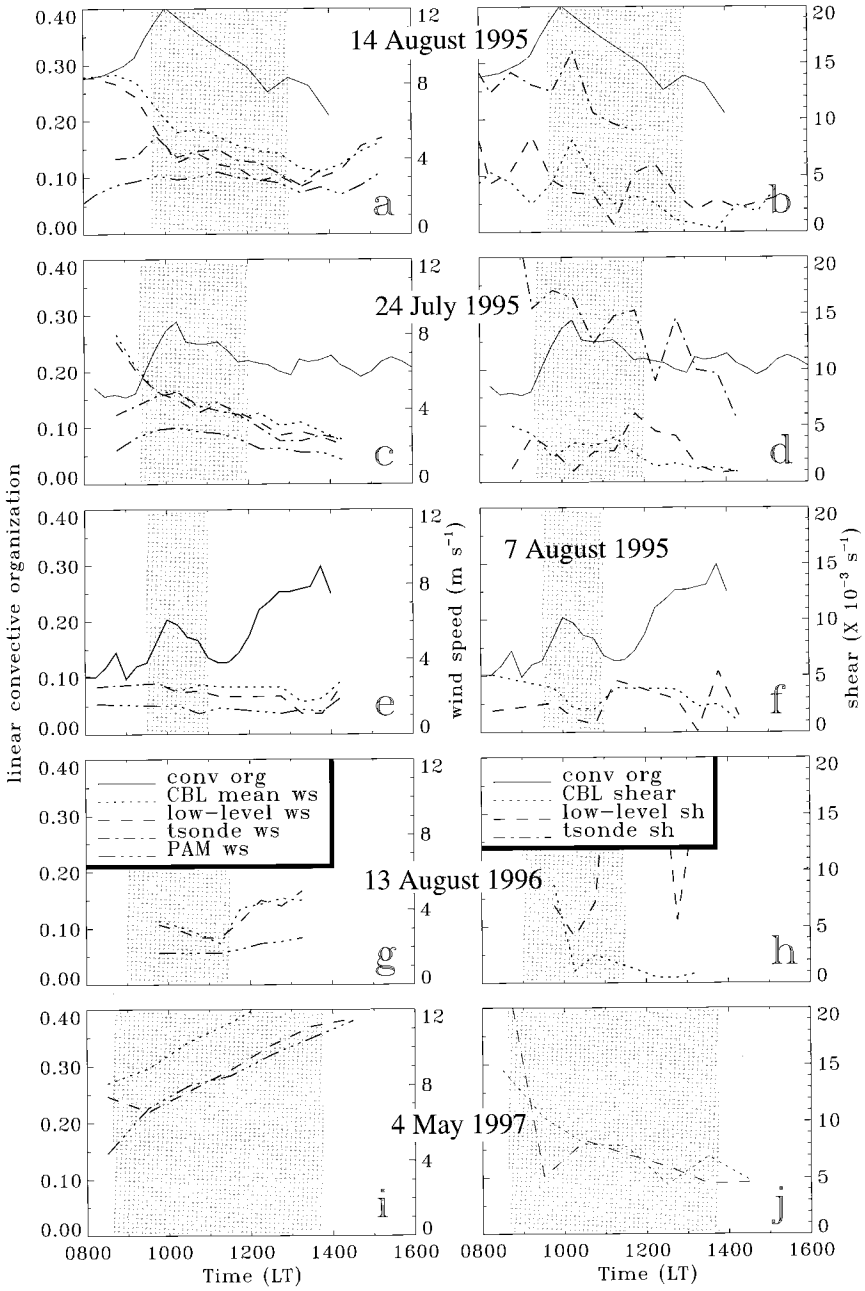

FIG. 10. Evolution of linear convective organization (solid lines where available) along with wind speed (m s^{-1}; left panels) and shear ($\times 10^{-3}$ s^{-1}; right panels). For 14 Aug 1995 (a), (b) and 24 Jul 1995 (c), (d) all parameters are included while 7 Aug 1995 (e), (f), 13 Aug 1996 (g), (h), and 4 May 1997 (i), (j) show only a subset of the parameters. The gray regions indicate the subjectively determined times of roll occurrences.

the first occurrence of rolls, there was not a well-defined mixed layer. The growth of a well-defined boundary layer, and thus a measurable z_i, occurred concurrently with the formation of rolls.

Buoyancy flux alone seemed to be the best indicator of when rolls would form (Fig. 12). The time series of buoyancy fluxes showed that rolls formed when the average $\overline{w'T_v'}$ was greater than 0.05 K m s^{-1} ($\sim$50 W m^{-2}) for all observed wind speeds. Note that the CBL (10-m PAM) wind speed was as low as 2.5 m s^{-1} (1.5 m s^{-1}) when rolls occurred on 7 August 1995 (Fig. 10e) and 13 August 1996 (Fig. 10g). If the CBL (Flux-PAM) winds were stronger than 5 m s^{-1} (3 m s^{-1}), as on 4 May 1997 (Fig. 10i), then the rolls formed with as little

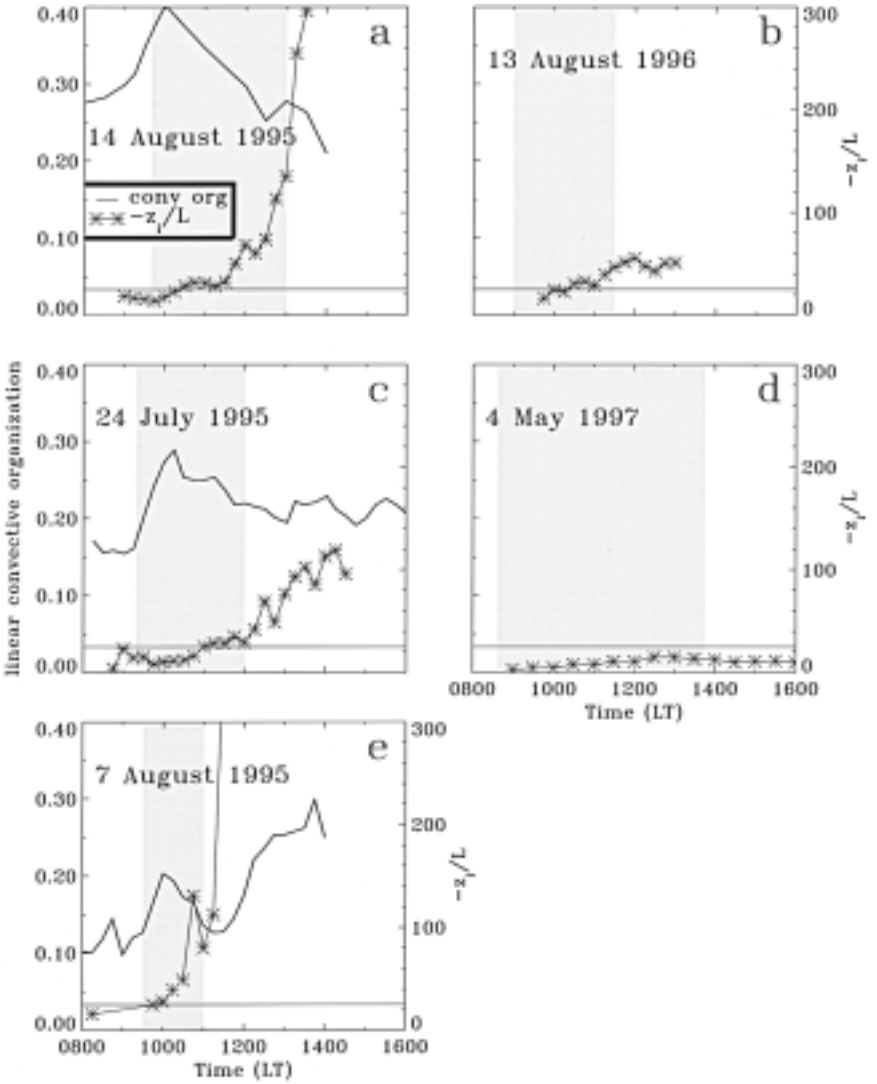

FIG. 11. Evolution of $-z_i/L$ (asterisks) along with linear convective organization (solid lines) on (a) 14 Aug 1995, (c) 24 Jul 1995, and (e) 7 Aug 1995 during SCMS. Objective analyses of linear convective organization were not available on (b) 13 Aug 1996 during LIFT and (d) 4 May 1997 during CASES-97. The gray regions indicate the subjectively determined times of roll occurrences. A solid line is drawn at $-z_i/L$ of 25 for reference.

buoyancy flux as 0.035 K m s^{-1} (~35 W m^{-2}). This threshold of buoyancy flux for roll formation was observed in all cases analyzed (a total of 13). A critical buoyancy flux for rolls is analogous to the critical conditions reported by Woodcock (1940) for soaring gulls and to the flux conditions for the onset of mesoscale cellular convection (Sheu and Agee 1977; Agee and Sheu 1978).

These results from Florida, Illinois, and Kansas suggest that (i) the first mode of organized boundary layer convection apparent in the radar data was two-dimensional horizontal convective rolls and (ii) these rolls formed when a critical value of buoyancy flux was achieved. This is consistent with past theoretical and laboratory work since the buoyancy flux may be considered a proxy for Rayleigh number, which could not be calculated with this dataset.

c. Roll dissipation

Hovmöller diagrams (Fig. 13) were used with the SCMS data as a means of providing a concise display of the evolution of the radar-observed convective features throughout the day. Time increases downward and decreasing range from CP-2 is along the ordinate. These diagrams were created by taking an average value of correlation coefficients (obtained from the correlation analysis described in section 2a) within rectangular regions. These regions were aligned along the roll axes and had a cross-roll width of 100 m. Also shown are

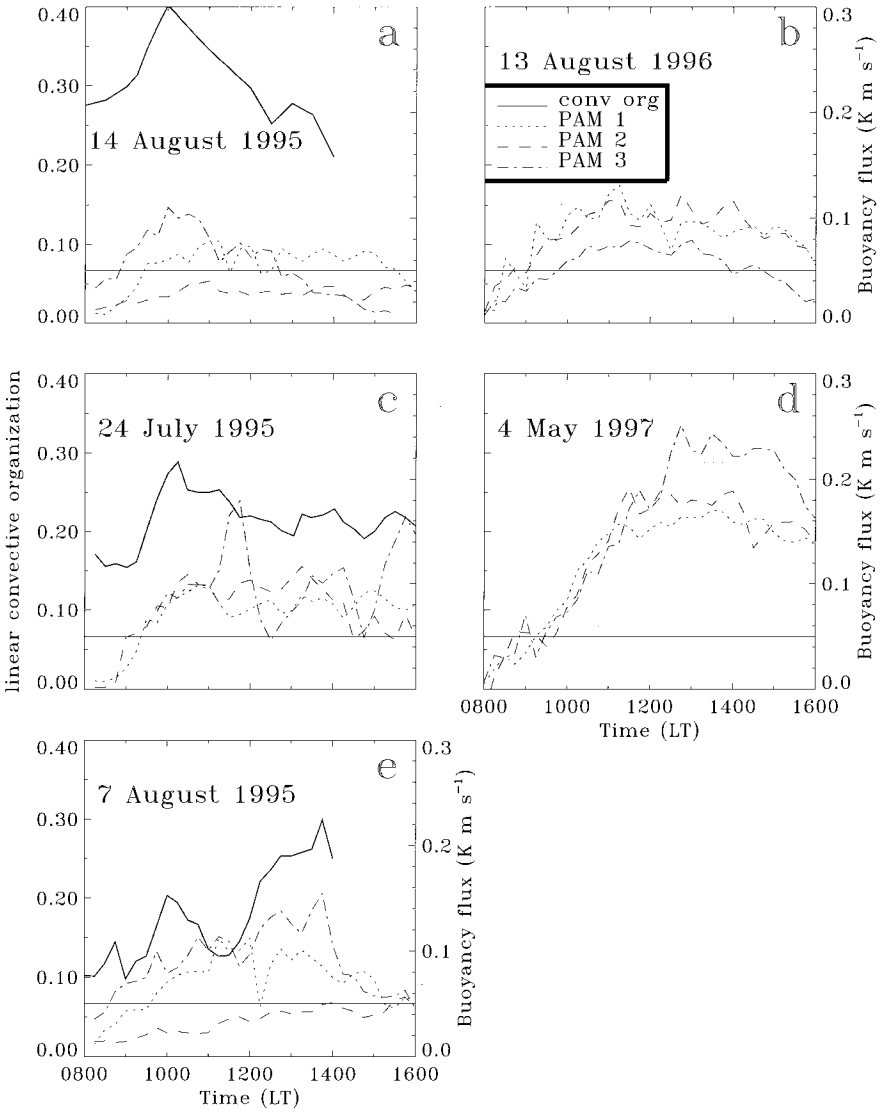

FIG. 12. Evolution of linear convective organization (solid lines when available) and buoyancy flux (K m s^{-1}) from three Flux-PAM stations on (a) 14 Aug 1995, (c) 24 Jul 1995, and (e) 7 Aug 1995 during SCMS, (b) 13 Aug 1996 during LIFT, and (d) 4 May 1997 during CASES-97. The gray regions indicate the subjectively determined times of roll occurrences. A solid line is drawn at 0.05 K m s^{-1} for reference.

the corresponding time series of linear convective organization, mean CBL wind speed, $-z_i/L$, and buoyancy flux, which were presented in Figs. 10, 11, and 12. The shaded regions in the right panels once again depict the subjectively determined times of roll occurrences. Figure 13a agrees with the radar time series of Fig. 3 in that there were no apparent convective motions until 0930 LT on 14 August 1995 when the buoyancy flux averaged from the three Flux-PAMs increased to 0.05 K m s^{-1} ($\sim$50 W m^{-2}). The linear convective features were tightly spaced until 1045 LT when the spacing nearly doubled. Note the vertically oriented maxima throughout most of the time series suggesting that the linear features were not propagating transverse to their axes on this day. The linear organization broke apart and formed larger-sized, less linear convective features after 1230 LT. Although $-z_i/L$ was not sufficient to explain the formation of rolls, it was linked to the dissipation of rolls. As $-z_i/L$ began to increase rapidly showing a dominance of convective instability, the convection became less two-dimensional. When $-z_i/L$ was greater than $\sim$25, the rolls became less organized (Figs. 11 and 13).

Similar to Fig. 13a both 24 July 1995 (Fig. 13c) and 7 August 1995 (Fig. 13e) started with little to no apparent convective features. Rolls formed by 0930 LT on

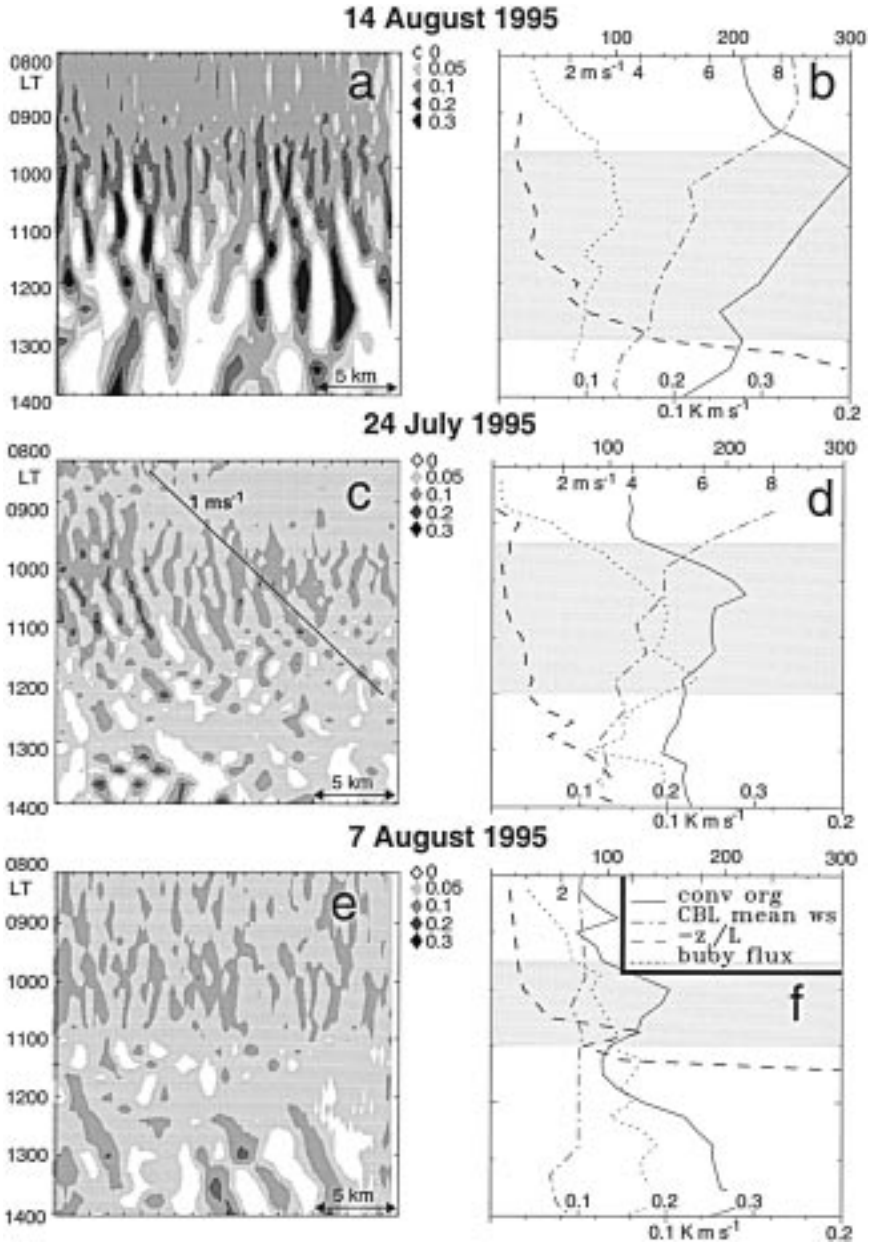

FIG. 13. Hovmöller diagrams (a), (c), and (e) with time increasing downward showing mean values of correlation coefficients at decreasing distance from CP-2 toward the right. The 1 m s^{-1} propagation speed line, typical for rolls, is shown in (c). The right panels (b), (d), and (f) show the corresponding time series of mean CBL wind speed (m s^{-1}; dotted–dashed line; scale on bottom of upper x axis), $-z_i/L$ (dashed line; scale on top upper x axis), buoyancy flux (K m s^{-1}; dotted line; scale on bottom lower x axis), and linear convective organization (solid line; scale on top of lower x axis). The shaded region corresponds with the subjectively determined times of roll occurrences.

both days when the buoyancy flux increased to 0.05 K m s^{-1}. On 24 July the rolls were more organized and linear. There was also a suggestion of eastward propagation of approximately 1 m s^{-1} toward the radar between 1000 and 1200 LT. The 1 m s^{-1} propagation line, which is typical for rolls (e.g., Faller 1965; LeMone 1973; Mason and Sykes 1982), is shown for reference. The rolls broke apart by 1200 LT as $-z_i/L$ increased above 25. On 7 August the rolls became less organized after 1030 LT as $-z_i/L$ rapidly increased. The wavelet analyses were not performed for the Flatland/LIFT project and therefore the Hovmöller diagrams were not obtained due to inconsistencies with the DOW1 radar. The wavelet analyses were not performed using the CASES-

97 S-Pol data because the S-band clear-air reflectivity field was noisy and did not depict clear-air motions as clearly as CP-2's X-band during SCMS (see section 2a).

It appeared that the existence (not the formation) of rolls was dependent upon the value of $-z_i/L$. During the day as the surface was heated, the boundary layer grew and the buoyancy dominated over shear. As the boundary layer became more convectively unstable, the rolls broke apart and became less two-dimensional. All SCMS examples and the Flatland/LIFT example show that as the value of $-z_i/L$ increased above 25, the linear convective organization decreased, consistent with past work (e.g., Grossman 1982; Weckwerth et al. 1997). For 4 May 1997 during CASES-97, however, $-z_i/L$ remained low throughout the day while the rolls broke apart. The reason for this is unknown.

d. Subsequent evolution

Although the Hovmöller diagrams were a useful tool for compressing the entire radar evolution into one figure, they did not clearly display the mode of convection if not linear. To identify the convective mode into which rolls evolved, one must look again at the radar images. On 14 August 1995 the rolls were well defined at 1025 LT (Fig. 3c) and they started to break apart at 1126 LT (Fig. 3d) and became unorganized convective elements by 1316 LT (Fig. 3e). Similarly on 24 July, the rolls were well defined at 1058 LT (Fig. 4c) and broke apart into unorganized convective features at 1328 LT (Fig. 4d). Also during CASES-97 on 4 May 1997 the linear features were well defined at 1217 LT and then broke apart into unorganized convective structures by 1441 LT (not shown). It is proposed that the cause of this evolution from rolls to unorganized convection was due to the relatively high magnitude of the winds. Referring back to the wind speeds that were shown in Fig. 10, note that on 14 August 1995 (Fig. 10a), 24 July 1995 (Fig. 10c), and 4 May 1997 (Fig. 10i) the mean CBL (10-m PAM) wind speeds were greater than 3 m s^{-1} (2 m s^{-1}) during the lifetime of the rolls.

In contrast to these three examples, on 7 August 1995 at 0945 LT the rolls were well defined (Fig. 5b) and then broke apart into open cellular convective features (e.g., Rothermel and Agee 1980; Agee 1987) by 1126 LT (Fig. 5d). A similar evolution occurred during the Flatland/LIFT project on 13 August 1996. The rolls were linear at 0914 LT (Fig. 6b), were breaking apart at 1110 LT (Fig. 6c), and became open cells by 1133 LT (Fig. 6d). The wind speeds on 7 August 1995 (Fig. 10e) and 13 August 1996 (Fig. 10g) were low (CBL winds <3 m s^{-1} and Flux-PAM winds <2 m s^{-1}) throughout the early part of the day when the rolls occurred. On these two days the rolls evolved toward cellular convection due to the minimal winds.

Thus these data suggested that (i) the value of the buoyancy flux (>50 W m^{-2} for all observed wind speeds and >35 W m^{-2} when CBL winds were >5 m s^{-1}) determined when rolls would form, (ii) the convective instability of the boundary layer determined when the rolls would become less linear ($-z_i/L > 25$), and (iii) the magnitude of wind speed predicted into which mode of boundary layer convection the rolls would evolve (if the CBL winds were less than 3 m s^{-1}, evolution was to open cells; if the CBL winds were greater than 3 m s^{-1}, evolution was to unorganized, random convection).

4. Roll orientation

Although the rolls were not well defined on 8 August 1995, it is a case that clearly shows the dominant variable influencing roll orientation. Figure 14 illustrates that the orientation of the linear features changed throughout the morning. At 1026 LT (Fig. 14a) and 1035 LT (Fig. 14b) the linear organization was northeast–southwest and after 1045 LT (Figs. 14c and 14d) northwest–southeast was the dominant orientation.

The wind profiler data for 8 August 1995 are shown in Fig. 15. Table 1 shows the changes in roll orientation and various direction measurements every half hour on 8 August 1995. Note that the strongest relationship existed between the roll orientation and the mean CBL wind direction. At 0947 LT the mean CBL wind direction was from 257°, consistent with the initial morning roll orientation (255°). When the roll orientation shifted to 280° at 1047 LT, the only direction measurement that had made a similar change was the mean CBL wind, which shifted to 279°. The roll orientation shifted farther to 300° at 1117 LT when the mean CBL wind direction was 299°. There was also a similar relationship between roll orientation and low-level wind direction although not as pronounced. There was not much variation in the shear direction or other directional measurements even when the orientation was changing substantially. It was clear that on 8 August 1995 the mean CBL wind direction was most influential in determining roll orientation. Although the other days analyzed did not exhibit such an obvious change in roll orientation, they also showed that roll orientation was consistent with the mean CBL wind direction. These results displaying the importance of CBL mean wind direction in defining roll orientation are similar to those of Malkus and Riehl (1964).

5. Summary and conclusions

The complete evolution of horizontal convective rolls was shown for three days during the SCMS, one day during the Flatland/LIFT project, and one day during CASES-97. All necessary observational platforms (e.g., radar to define roll occurrences, Flux-PAM stations to measure surface layer fluxes, and profilers to measure both boundary layer winds and boundary layer depth) were utilized when available to provide a description of the convective features, as well as the corresponding environmental parameters.

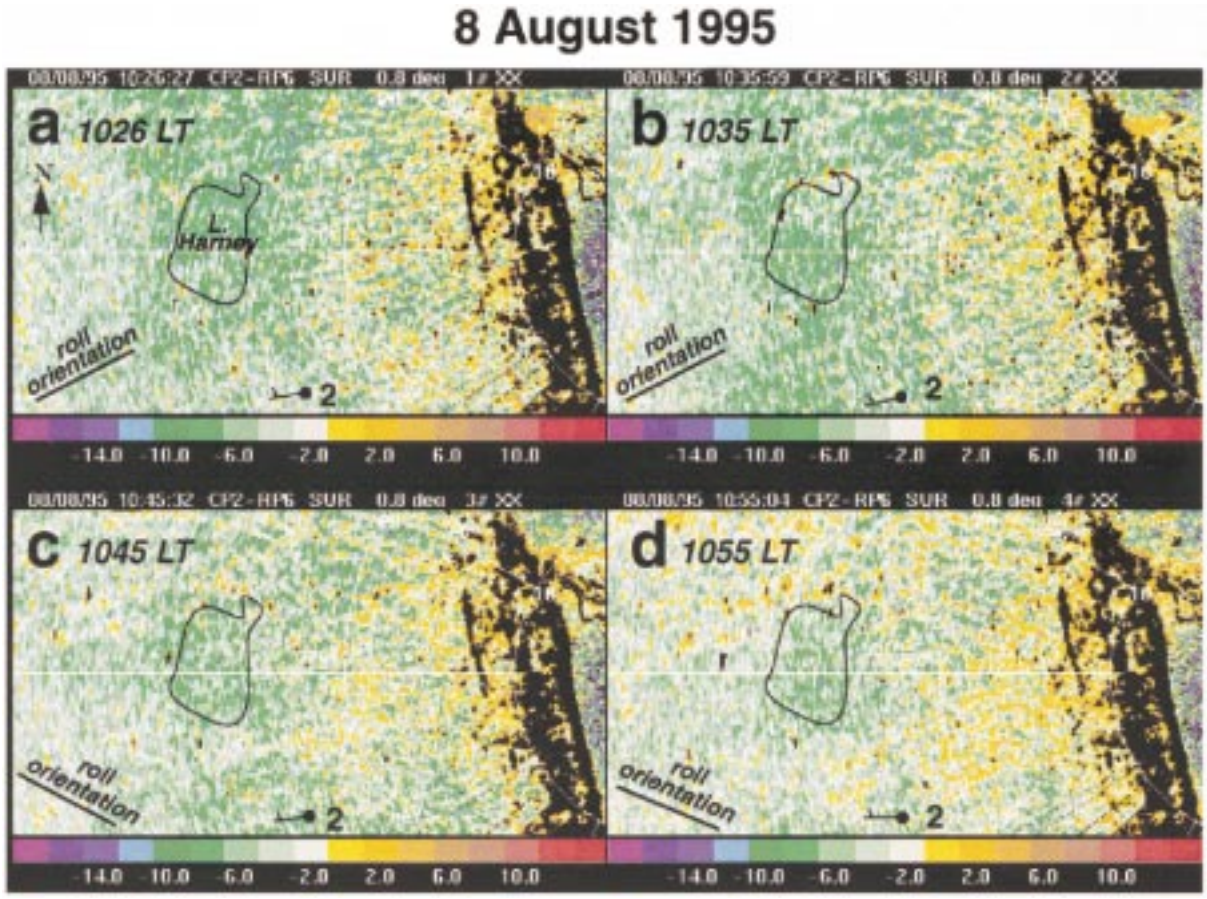

FIG. 14. The CP-2 X-band radar reflectivity data (dBZ_e) on 8 Aug 1995 showing a change in the orientation of the rolls between (a) 1026, (b) 1035 and (c) 1045, (d) 1055 LT during SCMS. Black regions indicate bad data. Lines indicating roll orientation are given in the lower-left corner of each panel. Wind measurements from Flux-PAM 2 are shown. Half barb is 2.5 m s^{-1}. Range rings are every 10 km; azimuth lines are every 30°. The outline of Lake Harney is shown for reference.

Data from various locations on all five days presented (14 August, 24 July, and 7 August 1995 in Florida; 13 August 1996 in Illinois; 4 May 1997 in Kansas) showed that *the first mode of organized boundary layer convection as observed by the radars was rolls.* Eight other days examined from SCMS supported this observation. Linear convection was observed even when the mean CBL (10-m Flux-PAM) wind speed values were as low as 2.5 m s^{-1} (1.5 m s^{-1}) and the shear measurements were minimal as well. This is consistent with previous theoretical and laboratory work, which showed that as the Rayleigh number in a fluid passes its critical value in the absence of vertical asymmetry in an initially motionless domain, two-dimensional convection will form.

Accurate measurements of the Rayleigh number were not available for this study but buoyancy flux measurements were used as a proxy. *In this study, the formation of rolls was dependent upon the magnitude of buoyancy flux.* For all observed wind speed and shear values, rolls formed with $\overline{w'T_v'} > 0.05$ K m s^{-1} (50 W m^{-2}). If the

TABLE 1. Roll orientation, Flux-PAM 10-m wind direction, mean CBL wind direction, CBL shear direction, low-level wind direction, low-level shear direction, and inversion-level wind direction on 8 Aug 1995 during SCMS.

Time (LT)	Orient. (°)	PAM dir. (°)	CBL mean dir. (°)	CBL sh. dir. (°)	Low-level mean dir. (°)	Low-level sh. dir. (°)	Inversion dir. (°)
0947	~255	204	257	311	244	300	268
1017	~255	221	269	329	255	311	277
1047	~280	230	279	355	258	313	297
1117	~280	235	293	335	281	344	312
1147	~300	249	299	353	277	350	318
1217	~300	269	305	337	297	3	303

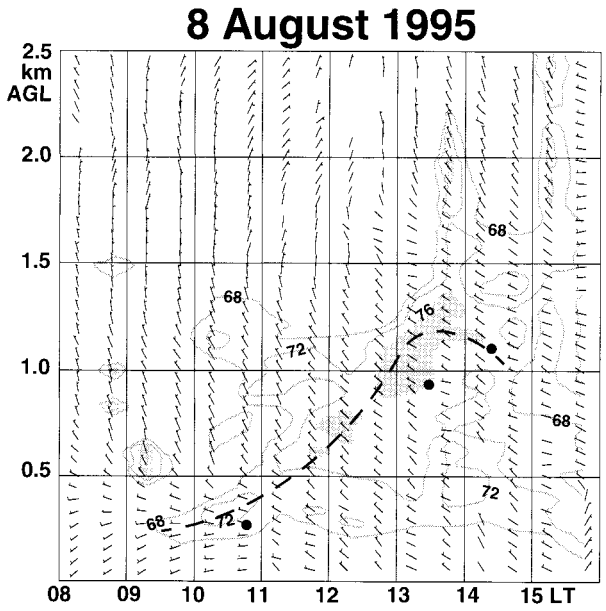

FIG. 15. Time series of wind profiler data on 8 Aug 1995 during SCMS. Full barbs are 5 m s^{-1} and half barbs are 2.5 m s^{-1}. Gray contours are range-corrected SNR every 4 dB starting at 68 dB with values greater than 76 dB shaded. The approximate height of the CBL, as determined from the maximum in SNR, is shown as the dashed line. The CBL height from three corresponding CLASS soundings are shown as black dots.

CBL (10-m Flux-PAM) wind speeds were greater than 3 m s^{-1} (2 m s^{-1}) with this dataset, then rolls formed with $\overline{w'T_v'}$ as low as 0.035 K m s^{-1} (35 W m^{-2}). The measure of convective instability in the boundary layer, $-z_i/L$, typically started at low values early in the morning and did not exceed a measurable threshold value prior to roll formation. This parameter, however, was influential for roll evolution. As the CBL deepened, the heat flux increased and the shear decreased. This led to a substantial increase in $-z_i/L$ throughout the day. Correspondingly, there was a decrease in the linear organization of the two-dimensional convective motions. Thus, *the decay of rolls was dependent upon* $-z_i/L$. Rolls became less organized as the boundary layer became more convectively unstable and $-z_i/L$ increased beyond approximately 25. In the cases presented herein, the rolls dissipated into either open cellular convection or unorganized, random convection.

The mode of boundary layer convection toward which the rolls evolved was dependent upon the wind speed. *If the rolls existed within an environment of low winds (CBL winds* $<$ *3 m* s^{-1} *and 10-m Flux-PAM winds* $<$ *2 m* s^{-1}*), they evolved into open cellular convection. If the rolls existed within an environment of relatively higher winds, they evolved into unorganized convective features, that is, random convection.*

The case study on 8 August clearly illustrates that mean CBL wind direction and possibly the low-level wind direction, rather than the inversion-level wind direction and all shear directions, were most influential in determining roll orientation. Thus, given the fact that (i) rolls were observed with this dataset within very low wind speed and shear environments and (ii) the wind speed and shear magnitudes themselves did not determine when rolls will form, it is believed that the winds were not necessary to force roll formation. Alternatively, during the onset of two-dimensional convection, it appeared that the wind played a role only in dictating the orientation of the rolls.

Acknowledgments. Numerous discussions with E. Agee (Purdue University), D. Kristovich (ISWS), R. Derickson (SDSMT), and C. Tong (Purdue University) were greatly appreciated. Detailed and extremely helpful reviews by P. LeMone (NCAR/MMM/ASP), P. Hildebrand (NCAR/ATD), R. Wakimoto (UCLA), N. Atkins (Lyndon State College), E. Agee, and one anonymous reviewer significantly improved the quality of this manuscript. C. Wade (NCAR/RAP) and J. Saez de la Adana (Metropolitan State University) were instrumental in collecting a valuable tethersonde dataset during SCMS. SCMS field support by and stimulating discussions with W. Abshire (UCAR/COMET) were a valuable contribution to this work. A great deal of assistance from J. Tuttle (NCAR/MMM) on the radar correlation analysis is appreciated. P. May (BMRC) and W. Angevine (NOAA/AL) were very helpful with the RASS data analyses. The radar data were obtained from B. Rilling (NCAR/ATD), the ISS data were obtained from E. Miller (NCAR/ATD), and surface station data were analyzed with software and data analysis support from G. MacLean (NCAR/ATD). Wind profiler data from CASES-97 were collected within the Argonne Boundary Layer Experiments array and were thus obtained from the Argonne National Laboratory. Special gratitude is bestowed upon the NCAR/ATD and ANL field support personnel who collected excellent datasets during SCMS, Flatland/LIFT, and CASES-97.

REFERENCES

Agee, E. M., 1987: Mesoscale cellular convection over the oceans. *Dyn. Atmos. Oceans,* **10,** 317–341.

——, and P.-J. Sheu, 1978: MCC and gull flight behavior. *Bound.-Layer Meteor.,* **14,** 247–251.

Angevine, W. M., A. B. White, and S. K. Avery, 1994: Boundary layer depth and entrainment zone characterization with a boundary layer profiler. *Bound.-Layer Meteor.,* **68,** 375–385.

——, A. W. Grimsdell, L. M. Hartten, and A. C. Delany, 1998: The Flatland boundary layer experiments. *Bull Amer. Meteor. Soc.,* **79,** 419–431.

Asai, T, 1970a: Stability of a plane parallel flow with variable vertical shear and unstable stratification. *J. Meteor. Soc. Japan,* **48,** 129–139.

——, 1970b: Three-dimensional features of thermal convection in a plane Couette flow. *J. Meteor. Soc. Japan,* **48,** 18–29.

——, 1972: Thermal instability of a shear flow turning the direction with height. *J. Meteor. Soc. Japan,* **50,** 525–532.

Brown, R. A., 1972: On the inflection point instability of a stratified Ekman boundary layer. *J. Atmos. Sci.,* **29,** 851–859.

——, 1980: Longitudinal instabilities and secondary flows in the planetary boundary layer: A review. *Rev. Geophys. Space Phys.*, **18,** 683–697.

Brümmer, B., S. Bakan, and H. Hinzpeter, 1985: KonTur: Observations of cloud streets and open cellular structures. *Dyn. Atmos. Oceans,* **9,** 281–296.

Chandrasekhar, S., 1961: *Hydrodynamic and Hydromagnetic Stability*. Oxford, 652 pp.

Christian, T. W., and R. M. Wakimoto, 1989: The relationship between radar reflectivities and clouds associated with horizontal roll convection on 8 August 1982. *Mon. Wea. Rev.,* **117,** 1530–1544.

Clark, T. L., T. Hauf, and J. P. Kuettner, 1986: Convectively forced internal gravity waves: Results from two-dimensional numerical experiments. *Quart. J. Roy. Meteor. Soc.,* **112,** 899–925.

Cohn, S., S. Mayor, C. Grund, T. Weckwerth, and C. Senff, 1998: The Lidars In Flat Terrain (LIFT) experiment. *Bull. Amer. Meteor. Soc.,* **79,** 1329–1343.

Deardorff, J. W., 1972: Numerical investigation of neutral and unstable planetary boundary layers. *J. Atmos. Sci.,* **29,** 91–115.

Doviak, R. J., and M. Berger, 1980: Turbulence and waves in the optically clear planetary boundary layer resolved by dual-Doppler radars. *Radio Sci.,* **15,** 297–317.

Faller, A. J., 1963: An experimental study of the instability of the laminar Ekman boundary layer. *J. Fluid Mech.,* **15,** 560–576.

——, 1965: Large eddies in the atmospheric boundary layer and their possible role in the formation of cloud rows. *J. Atmos. Sci.,* **22,** 176–184.

Fankhauser, J. C., N. A. Crook, J. Tuttle, L. J. Miller, and C. G. Wade, 1995: Initiation of deep convection along boundary layer convergence lines in a semitropical environment. *Mon. Wea. Rev.*, **123,** 291–313.

Ferrare, R. A., J. L. Schols, E. W. Eloranta, and R. Coulter, 1991: Lidar observations of banded convection during BLX83. *J. Appl. Meteor.,* **30,** 312–326.

Garratt, J. R., 1992: *The Atmospheric Boundary Layer*. Cambridge University Press, 316 pp.

Goldstein, R. J., and D. J. Graham, 1969: Stability of a horizontal fluid layer with zero shear boundaries. *Phys. Fluids,* **12,** 1133–1137.

Grossman, R. L., 1982: An analysis of vertical velocity spectra obtained in the BOMEX fair-weather, trade-wind boundary layer. *Bound.-Layer Meteor.,* **23,** 323–357.

Horst, T. W., and J. C. Weil, 1994: How far is far enough? The fetch requirements for micrometeorological measurement of surface fluxes. *J. Atmos. Oceanic Technol.,* **11,** 1018–1025.

——, and S. P. Oncley, 1995: Flux-PAM measurement of scalar fluxes using cospectral similarity. Preprints, *Ninth Symp. on Meteorological Observations and Instrumentation,* Charlotte, NC, Amer. Meteor. Soc., 495–500.

Keeler, R. J., B. W. Lewis, and G. R. Gray, 1989: Description of NCAR/FOF CP-2 meteorological Doppler radar. Preprints, *24th Conf. on Radar Meteorology,* Tallahassee, FL, Amer. Meteor. Soc., 589–592.

Kelly, R. D., 1982: A single Doppler radar study of horizontal-roll convection in a lake-effect snow storm. *J. Atmos. Sci.,* **39,** 1521–1531.

——, 1984: Horizontal roll and boundary-layer interrelationships observed over Lake Michigan. *J. Atmos. Sci.,* **41,** 1816–1826.

Khanna, S., and J. G. Brasseur, 1998: Three-dimensional buoyancy- and shear-induced local structure of the atmospheric boundary layer. *J. Atmos. Sci.,* **55,** 710–743.

Krishnamurti, R., 1970: On the transition to turbulent convection. Part 1. The transition from two- to three-dimensional flow. *J. Fluid Mech.,* **42,** 295–307.

Kristovich, D. A. R., 1993: Mean circulations of boundary-layer rolls in lake-effect snow storms. *Bound.-Layer Meteor.,* **63,** 293–315.

——, N. F. Laird, M. R. Hjelmfelt, R. G. Derickson, and K. Cooper. 1999: Transitions in boundary layer meso-γ convective structures: An observational case study. *Mon. Wea. Rev.,* in press.

Kuettner, J. P., 1959: The band structure of the atmosphere. *Tellus,* **2,** 267–294.

——, 1971: Cloud bands in the earth's atmosphere. *Tellus,* **23,** 404–425.

Kuo, H. L., 1963: Perturbations of plane Couette flow in stratified fluid and origin of cloud streets. *Phys. Fluids,* **6,** 195–211.

Lauritsen, D. K., Z. Malekmadani, C. Morel, and R. McBeth, 1987: The Cross-chain Loran Atmospheric Sounding System (CLASS). Preprints, *Sixth Symp. on Meteorological Observations and Instrumentation,* New Orleans, LA, Amer. Meteor. Soc., 265–269.

LeMone, M. A., 1973: The structure and dynamics of horizontal roll vortices in the planetary boundary layer. *J. Atmos. Sci.,* **30,** 1077–1091.

Lilly, D. K., 1966: On the instability of Ekman boundary flow. *J. Atmos. Sci.,* **23,** 481–494.

Lutz, J., B. Rilling, J. Wilson, T. Weckwerth, and J. Vivekanandan, 1997: S-Pol after three operational deployments, technical performance, siting experiences, and some data examples. Preprints, *28th Int. Conf. on Radar Meteorology,* Austin, TX, Amer. Meteor. Soc., 286–287.

Malkus, J. S., and H. Riehl, 1964: Cloud structure and distributions over the tropical Pacific Ocean. *Tellus,* **16,** 275–287.

Malkus, W. V. R., 1954: Discrete transitions in turbulent convection. *Proc. Roy. Soc. London,* **225A,** 185–195.

Mason, P. J., and R. I. Sykes, 1982: A two-dimensional numerical study of horizontal roll vortices in an inversion capped planetary boundary layer. *Quart. J. Roy. Meteor. Soc.,* **108,** 801–823.

Militzer, J. M., M. C. Michaelis, S. R. Semmer, K. S. Norris, T. W. Horst, S. P. Oncley, A. C. Delany, and F. V. Brock, 1995: Development of the prototype PAM III/Flux-PAM surface meteorological station. Preprints, *Ninth Symp. on Meteorological Observations and Instrumentation,* Charlotte, NC, Amer. Meteor. Soc., 490–494.

Miller, E. R., and A. C. Riddle, 1994: TOGA COARE integrated sounding system data report. Vol. 1A. NCAR, 61 pp. [Available from Atmospheric Technology Division, NCAR, P.O. Box 3000, Boulder, CO 80307-3000.]

Miura, Y., 1986: Aspect ratios of longitudinal rolls and convection cells observed during cold air outbreaks. *J. Atmos. Sci.,* **43,** 26–39.

Moeng, C.-H., and P. P. Sullivan, 1994: A comparison of shear- and buoyancy-driven planetary boundary layer flows. *J. Atmos. Sci.,* **51,** 999–1022.

Parsons, D., and Coauthors, 1994: The integrated sounding system: Description and preliminary observations from TOGA COARE. *Bull. Amer. Meteor. Soc.,* **75,** 553–567.

Rabin, R. N., P. J. Stadler, D. J. Stensrud, and M. Gregory, 1990: Observed effects of landscape variability on convective clouds. *Bull. Amer. Meteor. Soc.,* **71,** 272–280.

Rayleigh, O. M., 1916: On convection currents in a horizontal layer of fluid, when the higher temperature is on the under side. *Philos. Mag. Ser.,* **6,** 529–546.

Rothermel, J., and E. M. Agee, 1980: Aircraft investigation of mesoscale cellular convection during AMTEX 75. *J. Atmos. Sci.,* **37,** 1027–1040.

Russell, R. W., and J. W. Wilson, 1996: Aerial plankton detected by radar. *Nature,* **381,** 200–201.

Schlüter, A., D. Lortz, and F. Busse, 1965: On the stability of steady finite amplitude convection. *J. Fluid Mech.,* **23,** 129–144.

Segal, M., R. W. Arritt, J. Shen, C. Anderson, and M. Leuthold, 1997: On the clearing of cumulus clouds downwind from lakes. *Mon. Wea. Rev.,* **125,** 639–646.

Sheu, P.-J., and E. M. Agee, 1977: Kinematic analysis and air-sea heat flux associated with mesoscale cellular convection during AMTEX 75. *J. Atmos. Sci.,* **34,** 793–801.

Stull, R. B., 1988: *An Introduction to Boundary Layer Meteorology*. Kluwer Academic, 666 pp.

Sykes, R. I., and D. S. Henn, 1989: Large-eddy simulation of turbulent sheared convection. *J. Atmos. Sci.,* **46,** 1106–1118.

Walter, B. A., 1980: Wintertime observations of roll clouds over the Bering Sea. *Mon. Wea. Rev.,* **108,** 2024–2031.

Weckwerth, T. M., J. W. Wilson, and R. M. Wakimoto, 1996: Thermodynamic variability within the convective boundary layer due to horizontal convective rolls. *Mon. Wea. Rev.,* **124,** 769–784.

——, ——, ——, and N. A. Crook, 1997: Horizontal convective rolls: Determining the environmental conditions supporting their existence and characteristics. *Mon. Wea. Rev.,* **125,** 505–526.

Wilson, J. W., R. D. Roberts, C. Kessinger, and J. McCarthy, 1984: Microburst wind structure and evaluation of Doppler radar for airport wind shear detection. *J. Climate Appl. Meteor.,* **23,** 898–915.

——, T. M. Weckwerth, J. Vivekanandan, R. M. Wakimoto, and R. W. Russell, 1994: Boundary layer clear-air radar echoes: Origin of echoes and accuracy of derived winds. *J. Atmos. Oceanic Technol.,* **11,** 1184–1206.

Woodcock, A. H., 1940: Convection and soaring over the open sea. *J. Mar. Res.,* **3,** 248–253.

——, 1942: Soaring over the open sea. *Sci. Mon.,* **55,** 226–232.

Wurman, J., J. Straka, E. Rasmussen, M. Randall, and A. Zahrai, 1995: Design and first results from a portable, pencil-beam, pulsed Doppler radar. Preprints, *27th Int. Conf. on Radar Meteorology,* Vail, CO, Amer. Meteor. Soc., 713–716.